

Accepted Manuscript

DMSO coordinated dioxidomolybdenum(VI) complexes chelated with 3-methoxybenzhydrazone related ligands: Synthesis, structural studies and *in vitro* cytotoxicity

T.M. Asha, M.R.P. Kurup

PII: S0277-5387(19)30292-X

DOI: <https://doi.org/10.1016/j.poly.2019.04.045>

Reference: POLY 13905

To appear in: *Polyhedron*

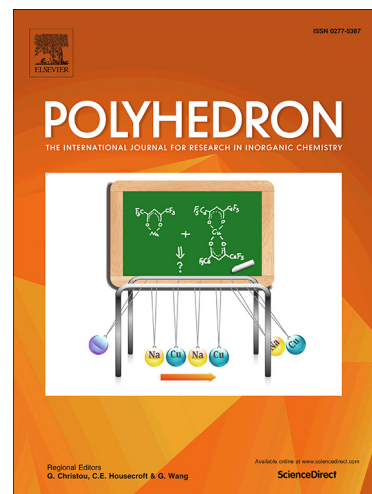
Received Date: 12 January 2019

Revised Date: 15 April 2019

Accepted Date: 24 April 2019

Please cite this article as: T.M. Asha, M.R.P. Kurup, DMSO coordinated dioxidomolybdenum(VI) complexes chelated with 3-methoxybenzhydrazone related ligands: Synthesis, structural studies and *in vitro* cytotoxicity, *Polyhedron* (2019), doi: <https://doi.org/10.1016/j.poly.2019.04.045>

This is a PDF file of an unedited manuscript that has been accepted for publication. As a service to our customers we are providing this early version of the manuscript. The manuscript will undergo copyediting, typesetting, and review of the resulting proof before it is published in its final form. Please note that during the production process errors may be discovered which could affect the content, and all legal disclaimers that apply to the journal pertain.



DMSO coordinated dioxidomolybdenum(VI) complexes chelated with 3-methoxybenzhydrazone related ligands: Synthesis, structural studies and *in vitro* cytotoxicity

T. M. Asha^a, M. R. P. Kurup^{a,b,*}

^aDepartment of Applied Chemistry, Cochin University of Science and Technology, Kochi 682 022, Kerala, India

^bDepartment of Chemistry, School of Physical Sciences, Central University of Kerala, Tejaswini Hills, Periyar, Kasargod 671 316, Kerala, India

Abstract: Three new DMSO coordinated dioxidomolybdenum(VI) complexes [MoO₂L^{3OMe}(DMSO)] (**1**), [MoO₂L^{4OMe}(DMSO)] (**2**) and [MoO₂L^{5OMe}(DMSO)] (**3**) (where, L^{3OMe} = 2-oxy-3-methoxybenzaldehyde-3-methoxy-benzhydrazonato, L^{4OMe} = 2-oxy-4-methoxybenzaldehyde-3-methoxybenzhydrazonato and L^{5OMe} = 2-oxy-5-methoxybenzaldehyde-3-methoxybenzhydrazonato) (Scheme 1) were synthesized by reacting [MoO₂(acac)₂] with the corresponding aroylhydrazone in presence of the solvent, DMSO and fully characterized. The various characterization techniques included elemental analysis, spectroscopic techniques (IR, electronic and ¹H NMR), thermogravimetric analysis and cyclic voltammetry. The molecular and crystal structures of **1**, **2** and **3** were determined by single crystal X-ray diffraction method. In all complexes the molybdenum atom displays a distorted octahedral geometry. In addition, the discussion on coordination geometries and non-covalent interactions were also supported using Hirshfeld surface analysis. The *in vitro* cytotoxicity of the aroylhydrazone ligands and their molybdenum complexes against lymphoma ascites cell line demonstrated that the complexes are more cytotoxic than their corresponding ligands.

Keywords: Molybdenum(VI) complex, DMSO, Elemental analysis, Hirshfeld surface analysis, Cytotoxicity, Lymphoma

Scheme 1

*Corresponding author at: Department of Chemistry, School of Physical Sciences, Central University of Kerala, Tejaswini Hills, Periyar, Kasargod, 671 316, India, E-mail address: mrpcusat@gmail.com, mrp@cukerala.ac.in (M.R.P. Kurup).

1. Introduction

Aroylhydrazones characterized by azomethine group ($RC=N-$) are excellent multidentate ligands that form a significant class of compounds in medicinal and pharmaceutical chemistry and are known to have biological applications due to their antibacterial [1-6], antifungal [3-6] and antitumor [7,8] activities. Moreover the incorporation of transition metals into these compounds [9] can lead to the enhancement of their biological property [10,11]. As one of the versatile element of the periodic table, spanning oxidation states of -2 to +6, molybdenum has drawn the attention of the coordination chemist in general [12-16]. At the present moment, the coordination chemistry of molybdenum has become a prospective area of research due to the significant enzymatic role played by molybdenum in biochemical reactions [17-19] especially in the oxidation of aldehydes, purines and sulfides [20].

In this context, the oxidomolybdenum complexes coordinated with tridentate ligands have drawn significant attention due to their similarity to the active site of majority of molybdoenzymes [12,21]. This enzymatic role of molybdenum in biological reactions has created a tremendous impetus in the syntheses of a number of model complexes mimicking oxotransferase molybdoenzymes [13,22-27]. Molybdenum(VI) Schiff base complexes with a *cis*- MoO_2 core are excellent enzyme model systems for this purpose. Moreover possessing an $Mo=O$ unit has been widely used in catalysis for numerous industrially important chemical reactions such as hydrogen generation [28], alkene epoxidation [29,30] and sulfide oxidation [31].

In spite of the synthesis of many molybdenum Schiff base complexes, there are few reports on the cytotoxicity of these complexes, though our group have reported the synthesis and *in vitro* cytotoxicity studies of dioxidomolybdenum(VI) complexes derived from an ONO donor aroylhydrazone with different donor auxiliary ligands [32]. In continuation of our previous study [32], the present study focuses on the effect of position of the methoxy substituent on the aldehydic part (keeping the hydrazide part constant) on their crystal structures and *in vitro*-cytotoxicity.

2. Results and discussion

2.1 Synthesis and characterization

The aroylhydrazones, H_2L^R ($R= 3OMe, 4OMe$ and $5OMe$) are soluble in both protic solvents such as MeOH and EtOH, as well as in aprotic solvents such as DMF and DMSO. The reaction of the aroylhydrazones with $[MoO_2(acac)_2]$ in 1:1 molar ratio in presence of DMSO yielded solid complexes corresponding to the general formula $[MoO_2L^R(DMSO)]$ ($R= 3OMe$ (**1**), $4OMe$ (**2**) and $5OMe$ (**3**)). The complexes are stable at room temperature and are insoluble in most of the inorganic solvents, but readily soluble in DMSO and DMF. The molar conductance values of

the complexes were measured in DMF (10^{-3} M) at room temperature and showed values within the range (5-10) Ω^{-1} cm² mol⁻¹ indicating their non-electrolytic nature in solution [33]. The aroylhydrazone ligands and their respective complexes were characterized by IR, ¹H NMR and UV-visible spectroscopic techniques along with thermal and cyclic voltammetric measurements.

2.2 IR spectra: The IR spectra of the aroylhydrazones, H₂L^{3OMe}, H₂L^{4OMe} and H₂L^{5OMe} exhibit medium and broad band centered at 3580, 3448 and 3468 cm⁻¹ respectively and are assigned to $\nu(\text{O-H})$ vibrations. Weak and sharp bands at 3184, 3226 and 3217 cm⁻¹ respectively corresponds to the $\nu(\text{N-H})$ vibrations. On the other hand sharp bands at 1645, 1624 and 1654 cm⁻¹ respectively are attributed to the $\nu(\text{C=O})$ vibrations [34].

The IR spectra of the complexes are mostly similar. The complexes do not exhibit ligand bands of $\nu(\text{O-H})$, $\nu(\text{N-H})$ and $\nu(\text{C=O})$ vibrations indicating the enolization and deprotonation of the aroyl hydrazones with concomitant coordination of the enolic and phenolic groups to the molybdenum atom, which is in accordance with the result obtained by X-ray crystallography [34]. Moreover the appearance of new C–O bands at 1251, 1296 and 1239 cm⁻¹ for complexes **1**, **2** and **3** suggest the tautomerisation of hydrazone ligands and coordination in the enolate form. The characteristic imine band in H₂L^{3OMe}, H₂L^{4OMe} and H₂L^{5OMe}, which exist at 1644, 1630 and 1647 cm⁻¹ respectively were found to have shifted to lower frequency of 1619, 1615 and 1643 cm⁻¹ for their corresponding complexes [35] indicating the coordination of azomethine nitrogen atom to the molybdenum ion [36]. Medium to strong band at about 1431-1499 cm⁻¹ for the free hydrazone ligands are assigned to phenolic $\nu(\text{C-O})$ stretch which undergoes a shift to lower frequency in the case of molybdenum complexes [37] suggesting that the phenolic oxygen atom also coordinate to molybdenum ion. Only a slight change is observed in the position of the bands in the 1046-1132 cm⁻¹ region which are assigned to $\nu(\text{N-N})$ stretch in the case of molybdenum complexes. The Mo=O stretching modes occurring as a pair of sharp and strong bands at 948 and 893 cm⁻¹; 901 and 853 cm⁻¹; 949 and 852 cm⁻¹ for the respective complexes **1**, **2** and **3** are assigned to the antisymmetric and symmetric stretching modes respectively. This is in accordance with the observation on similar complexes [32,37,38]. The infrared spectral assignments for the dioxidomolybdenum complexes **1-3** are presented in the Table S1 of the supporting information.

2.3 ¹H NMR spectra: The ¹H NMR spectra of the hydrazone ligands, H₂L^{3OMe-5OMe} and their molybdenum(VI) complexes were recorded in DMSO. The ¹H NMR spectra of the free aroylhydrazones exhibited a singlet in the downfield region of the spectrum at $\delta = 11.972$ - 12.120 ppm due to the iminolic proton (HN–N). The phenolic OH proton (OH_{phenolic}) resonates at $\delta = 10.746$ - 11.614 ppm and H_{azomethine}–C=N at $\delta = 8.550$ - 8.695 ppm.

Upon complexation, the OH and NH proton signals disappeared indicating the deprotonation of phenolic OH and NH and subsequent coordination of oxygen atom of the phenolic group and azomethine nitrogen atom to molybdenum atom. The participation of the azomethine nitrogen in complexation is signaled by an appreciable downfield shift of the azomethine proton signal. All the aromatic proton signals of the aroylhydrazones and their Mo complexes were observed in the expected region of $\delta = 6.504\text{--}7.648$ ppm. All the three complexes exhibit resonance peaks corresponding to the coordinated DMSO molecule at $\delta = 2.546\text{--}2.565$ ppm which are tabulated in Table S2.

2.4 Electronic spectra: Electronic spectra of the aroylhydrazones and their molybdenum complexes were recorded in DMF as well as in DMSO and the spectral characteristics of the compounds are listed in Table S3(a) and S3(b). The electronic spectra of the complexes **1-3** exhibit strong absorptions between 420-452 nm which is believed to originate from the charge transfer transition of the type $L \rightarrow Mo(d\pi)$ between the highest occupied ligand molecular orbital and the lowest empty d orbital of molybdenum [38]. In addition to that, complexes **1-3** exhibit strong absorption between 300-330 nm regions owing to the intraligand transitions [38]. Absence of bands due to d-d transition supports the existence of Mo(VI) ion [39].

2.5 Thermogravimetric analysis: Thermal behavior of the complexes **1**, **2** and **3** were studied using thermogravimetric analysis and the experiments were carried out under nitrogen atmosphere in the temperature range 35–900 °C at a heating rate of 10 °C min⁻¹. The samples were purged by a stream of dry nitrogen flowing at 20 mL min⁻¹. The thermal curves of all the three complexes are presented in Figure 1.

The TGA curves of the complexes reveal that all the complexes are stable upto a temperature of 150 °C and undergo decomposition at two well defined stages (Table 1). The loss of weakly coordinated DMSO molecule occurred between the temperature range of 200-240 °C, 150-210 °C and 170-205 °C for complexes **1**, **2** and **3** respectively. With further elevation in temperature, the second stage of decomposition took place in the temperature range of 270-290 °C, 270-310 °C and 270-310 °C for **1**, **2** and **3** corresponding to the loss of (CH₃O-C₆H₄-CONN) moiety formed by the dissociation of the hydrazone ligand at the –C=N– bond. Decomposition continues until the final residue MoO₃ is left which was identified by qualitative analysis.

Figure 1

Table 1

2.6 PXRD analysis: Powder diffraction data revealed the isostructurality of the molybdenum complexes **1-3**. The PXRD patterns of complexes **1-3** is depicted in Figure 2.

Figure 2

2.7 Electrochemical studies: The redox behavior of the aroylhydrazones and their molybdenum complexes were examined in DMF solution by cyclic voltammetry at platinum electrode with 0.1 M tetraethylammonium perchlorate (TEAP) as the supporting electrolyte. The CV data is tabulated in Table 2. The aroylhydrazones, H_2L^{3OMe} , H_2L^{4OMe} and H_2L^{5OMe} exhibit an irreversible one reductive peak around -0.458 V, 1.233 V and 1.479 V respectively.

The CV trace of complex **1** portrayed two irreversible reductive responses within the potential window of -0.894 to -0.331 V, which can be attributed to the Mo^{VI}/Mo^V and Mo^V/Mo^{VI} processes, respectively [17,40]. Whereas complexes **2** and **3** exhibited only one irreversible reductive peak around -1.190 V and -1.198 V respectively owing to the Mo^{VI}/Mo^V process. The dearth of anodic response in the CV traces of the complexes **1-3** even at a higher scan rate can be attributed to the rapid decomposition of the reduced species [41].

Table 2

2.8 Crystallographic description of the complexes

The crystal data of complexes **1-3** are presented in Table 3. The molecular structures and atom numbering schemes for the complexes **1-3** are shown in Figure 3 and the selected bond distances and bond angles are presented in Table 4. Crystal structures of the three complexes revealed that in all complexes, the aroylhydrazones act as a tridentate ligand bonding through its imine nitrogen, N(1), phenoxy oxygen, O(1) and the hydroxyl oxygen, O(3) from the enolized carbonyl group forming five and six membered chelate ring around *cis*- MoO_2 centre. The chelate rings form bite angles O(1)–Mo(1)–N(1) ($82.093(8)^\circ$ for **1**, $80.716(6)^\circ$ for **2** and $82.093(6)^\circ$ for **3**) and O(3)–Mo(1)–N(1) ($71.755(8)^\circ$ for **1**, $72.300(6)^\circ$ for **2** and $71.763(7)^\circ$ for **3**). Molybdenum ion features a distorted octahedral geometry with an NO_5 coordination sphere, where the imine nitrogen, phenoxy oxygen, enolic oxygen and one of the oxido oxygen atom O(5) of the dioxidomolybdenum unit occupying the equatorial position. On the other hand, the apical positions of the octahedron are occupied by the other oxido oxygen atom O(6) and the oxygen atom of the coordinated DMSO molecule O(7).

Table 3

Figure 3

Table 4

The values of the Mo=O bond lengths, 1.7061(2) and 1.6943(2) Å for **1**, 1.7183(2) and 1.6976(1) Å for **2** and 1.7072(2) and 1.6933(16) Å for **3** are similar for other *cis*- MoO_2 complexes

[15,40-43] and the Mo–O, Mo–N and N–N bond lengths are also found to be within the Mo(L) fragment. In Mo complexes, based on the MoO₂²⁺ core it is expected, due to the *trans* effect, the Mo–D (D = donor atom of the coordinated ligand) bonds positioned *trans* to the oxygen atoms of the MoO₂²⁺ core are longer than the remaining ones. Thus, the longer Mo–O(DMSO) distance is well expected for this type of complexes. The C–O bond distances C(8)–O(3) for the complexes (1.3251(4) Å for **1**, 1.3343(7) Å for **2** and 1.3298(3) Å for **3**) were found to be nearer to a C–O single bond (1.42 Å) than to a C–O double bond distance (1.16 Å).

Another fascinating observation is that the Mo atom in the molecular structures of complexes **1-3** shows a displacement towards the apical oxido oxygen atom, O(6) by around 0.2 Å from the O1/N1/O3/O5 basal plane.

Molecular structures of all the complexes exhibited a common non-classical intermolecular hydrogen bonding interaction, where the aldehydic proton, H(7) is involved in intermolecular hydrogen bonding interaction with oxido oxygen atom, O(6). Similarly complexes, **1** (Figure 4) and **2** (Figure S1) exhibit an intermolecular hydrogen bonding interaction between aromatic proton of the salicylaldehyde and the other oxido oxygen atom, O(5). Crystal structure of complex **3** (Figure S2) exhibited two bifurcated hydrogen bonding interactions where both the oxido oxygen atom, O(5) and O(6) are involved in bonding with methyl proton of coordinated DMSO [H(18A)] and aromatic proton H(2) of salicylaldehyde; and methyl proton of coordinated DMSO respectively. Whereas in complex **2**, the methyl protons of DMSO [H(18A) and H(18C)] shows intermolecular hydrogen bonding interaction with methoxy oxygen atom, O(4) and enolic oxygen atom, O(3) of the benzhydrazide moiety. Crystal structures of **1-3** are deficient of any classical hydrogen bonding interactions. The interaction parameters for the hydrogen bonding interactions are tabulated in Table S4.

Figure 4

In complexes **1** and **3**, the six membered chelate ring involving molybdenum atom, Mo1/O1/C1/C6/C7/N1 is puckered with a puckering amplitudes of $Q = 0.3194(18)$ Å, $\varphi = 197.8(5)^\circ$ and $Q = 0.2971(16)$ Å, $\varphi = 25.7(4)^\circ$ respectively. Furthermore complexes **1-3** do not exhibit any π - π interactions.

2.9 Hirshfeld surface analysis

The intermolecular interactions in the crystal structures of the complexes **1-3** were visualized with the help of Crystal Explorer 17.5 [44]. The Hirshfeld surface of the complexes **1-3** are shown in Figure 5 that have been mapped over a 3D d_{norm} , shape index and curvedness. A measure of globularity (G) and asphericity (Ω) [45] were also made (Table S2). Globularity values for all the

complexes are in the range 0.680–0.691 which shows that all of them deviate from spherical surface [46].

Figure 5

Asphericity (Ω) values (Table S5) are a measure of anisotropy of objects and it was found to be 0.198-0.216 indicating their deviation from symmetry [47]. Graphical plots of the molecular Hirshfeld surfaces mapped with d_{norm} employs a red–white–blue color scheme, where the white surface indicates contacts with distance equal to the sum of van der Waals radii, whereas the red and blue color indicates distance shorter (in close contact) or longer (distance contact) than van der Waals radii, respectively [48]. The medium red color spots in the Hirshfeld surface mapped with d_{norm} of the complexes **1-3** display the major C–H \cdots O interaction due to the presence of non-classical hydrogen bonding interaction involving the complexes in the asymmetric unit (Figure 6).

Shape index patterns give a perception about the various π - π stacking interactions present in the complex which appears as “bow-tie” patterns. Dearth of such patterns in the shape index surface of complexes (Figure 6) indicate the absence of any π - π stacking interactions in the crystals of these complexes substantiating the results obtained from the crystal data [49,50]. The curvedness is a measure of the shape of the surface area of the molecule. The flat areas of the surface correspond to low values of curvedness, while sharp curvature areas correspond to high values of curvedness and usually tend to divide the surface into patches, indicating interactions between neighboring molecules. The large flat region delineated by a blue outline refer to the $\pi\cdots\pi$ stacking interactions. Therefore the curvedness of the complexes (Figure 6) also reveals that $\pi\cdots\pi$ stacking interactions are absent in these complexes [50,51].

The combination of d_e and d_i in the form of a 2D fingerprint plot provides a summary of intermolecular contacts in the crystal and are in complement to the Hirshfeld surfaces. 2D fingerprint plots of Hirshfeld surface for the complexes and the relative contributions of different interactions overlapping in the full fingerprint plots are shown in Figure 7. Complementary regions are visible in the fingerprint plots where one molecule act as donor ($d_e > d_i$) and the other as an acceptor ($d_e < d_i$). Decomposition enables separation of contributions from different interactions which overlap in full fingerprint plots. The decomposition of fingerprint plot shows that the non-directional H \cdots H/H \cdots H interactions have the highest contribution (40.9% in **1**, 40.3% in **2** and 41.6% in **3**) of the total Hirshfeld surface. Despite the high share of this interaction, its role in the stabilization of structure is quite small in magnitude because this interaction is between the same species [52]. The O \cdots H/H \cdots O intermolecular interactions appear as distinct spikes in the 2D fingerprint plots. The proportions of this interaction are 32.7, 32.4, and 33% of the Hirshfeld surfaces for each molecule of **1**, **2** and **3**, respectively. No significant C–H \cdots π interactions are

observed in these complexes while the C...H close contacts are 14.4%, 16.4%, and 14.6% in **1**, **2**, and **3**, respectively. Relative contributions from all the major interactions to the Hirshfeld surface are specified in Figure 8.

Figure 6

Figure 7

Figure 8

2.10 *In vitro* cytotoxicity

In vitro cytotoxicity of the complexes **1-3** were evaluated using Dalton's lymphoma ascites cell line (DLA). The results of the investigation (Table 5) demonstrate a dose-dependent (10, 25, 50, 100 and 200 µg/mL) behavior for all the studied complexes against the aforementioned cell line.

The free aroylhydrazones showed very low cytotoxicity compared to their corresponding molybdenum complexes showing the essential role made by the metal, molybdenum in facilitating the potency of these complexes. The potency of the compound to kill the cells followed the order **3>1>2** (Figure 9) indicating that complex **3** is the more effective complex in controlling the growth of DLA cell lines among the three complexes. This may be attributed to the difference in the position of the methoxy substituent of the salicylaldehyde part of these complexes.

Difference in the cell lines and treatment duration made it difficult for us to compare the cytotoxicity effect of the present complexes with that of the other molybdenum complexes other than those previously reported by our group [32].

Table 5

Figure 9

3. Experimental section

3.1 Materials

All chemicals used were procured commercially and used without subsequent purification. 2-Hydroxy-5-methoxybenzaldehyde, 3-methoxybenzhydrazide, [MoO₂(acac)₂], were obtained from Sigma Aldrich, 2-hydroxy-3-methoxybenzaldehyde and 2-hydroxy-5-methoxybenzaldehyde from Alfa Aesar. Solvents methanol, DMF and DMSO were purchased from Spectrochem.

3.2 Instrumentation and characterization procedures

Elemental analyses were carried out using a Vario EL III CHNS analyser. Infrared spectra were recorded as KBr pellets on a JASCO FT-IR-5300 spectrometer in the range 4000-400 cm⁻¹.

Electronic spectra were recorded using a Thermo Scientific Evolution 220 model UV-vis spectrophotometer in the 200-900 nm range. Molar conductivities of the complexes in DMF solutions (10^{-3} M) at room temperature were measured using a Systronic model 303 direct reading conductivity meter. The ^1H NMR spectra were recorded using a Bruker AMX 400 FT-NMR Spectrometer using TMS as internal standard at ambient temperature. Thermogravimetric (TG) analysis of the complexes was carried out by heating in a nitrogen gas at a rate of $10\text{ }^\circ\text{C}$ per minute on a Perkin Elmer Pyris TGA thermobalance. Electrochemical measurements were carried out using a CH 6017B instrument using Pt working electrode, a Pt auxiliary electrode and Ag/AgCl reference electrode. Cyclic voltammograms were recorded in DMF containing 0.1 M TEAP (tetraethylammonium perchlorate) as a supporting electrolyte and a 5×10^{-4} M complex solution deoxygenated by bubbling with nitrogen gas before use. The X-ray powder diffraction patterns of complexes 1-3 were recorded on a Bruker AXS D8 Advance diffractometer.

3.3 Synthesis

3.3.1. Syntheses of the aroylhydrazones

2-Hydroxy-3-methoxybenzaldehyde-3-methoxybenzhydrazone ($\text{H}_2\text{L}^{3\text{OMe}}$): 2-Hydroxy-3-methoxybenzaldehyde, 0.152 g (1.0 mmol) was dissolved in 20 ml methanol. The solution was then added to a methanolic solution of 0.166 g (1.0 mmol) of 3-methoxybenzhydrazide. The reaction mixture was refluxed for 3 h resulting in a light yellow colored solution. A precipitate was formed when the solution was allowed to cool at room temperature overnight. The yellow precipitate obtained was filtered, washed with methanol and dried in air.

Yield: 0.18 g, 63%. Anal.Cal. for $\text{C}_{16}\text{H}_{16}\text{N}_2\text{O}_4$ (300.31 g mol^{-1}); C, 63.99; H, 5.37; N, 9.33. Found: C, 63.92; H, 5.29; N, 9.35. IR (KBr) ν_{max} , cm^{-1} : $\nu(\text{O-H})$ 3580(m), $\nu(\text{N-H})$ 3184(m), $\nu(\text{C=O})$ 1645(s). ^1H NMR (400 MHz, $\text{DMSO-}d_6$, Me_4Si , ppm) δ : 3.806 (s, 3H, methoxy), 3.824 (s, 3H, methoxy), 6.851-7.520 (m, 7H, aromatic), 8.645 (s, 1H, HC=N), 10.993 (s, 1H, OH group), 12.081 (s, 1H, NH group). UV/vis (DMF) λ_{max} , nm (ϵ , $\text{L mol}^{-1}\text{ cm}^{-1}$): 302 (15600).

Similar procedure was applied for the preparation of $\text{H}_2\text{L}^{4\text{OMe}}$ and $\text{H}_2\text{L}^{5\text{OMe}}$.

2-Hydroxy-4-methoxybenzaldehyde-3-methoxybenzohydrazone, ($\text{H}_2\text{L}^{4\text{OMe}}$): Yield: 0.20 g, 67%. Anal.Cal. for $\text{C}_{16}\text{H}_{16}\text{N}_2\text{O}_4$ (300.31 g mol^{-1}); C, 63.99; H, 5.37; N, 9.33. Found: C, 63.95; H, 5.32; N, 9.37. IR (KBr) ν_{max} , cm^{-1} : $\nu(\text{O-H})$ 3580(m), $\nu(\text{N-H})$ 3184(m), $\nu(\text{C=O})$ 1645(s). ^1H NMR (400 MHz, $\text{DMSO-}d_6$, Me_4Si , ppm) δ : 3.834 (s, 3H, methoxy), 3.778 (s, 3H, methoxy), 6.504-7.513 (m, 7H, aromatic), 8.550 (s, 1H, HC=N), 11.614 (s, 1H, OH group), 11.972 (s, 1H, NH group). UV/vis (DMF) λ_{max} , nm (ϵ , $\text{L mol}^{-1}\text{ cm}^{-1}$): 331 (84125).

2-Hydroxy-5-methoxybenzaldehyde-3-methoxybenzohydrazone, (H_2L^{5OMe}): Yield: 0.17 g, 57%. Anal.Cal. for $C_{16}H_{16}N_2O_4$ ($300.31 \text{ g mol}^{-1}$); C, 63.99; H, 5.37; N, 9.33. Found: C, 63.85; H, 5.41; N, 9.31. IR (KBr) ν_{\max} , cm^{-1} : $\nu(\text{O-H})$ 3580(m), $\nu(\text{N-H})$ 3184(m), $\nu(\text{C=O})$ 1645(s). $^1\text{H NMR}$ (400 MHz, $\text{DMSO-}d_6$, Me_4Si , ppm) δ : 3.798 (s, 3H, methoxy), 3.901 (s, 3H, methoxy), 6.922-7.589 (m, 7H, aromatic), 8.695 (s, 1H, HC=N), 10.746 (s, 1H, OH group), 12.120 (s, 1H, NH group). UV/vis (DMF) λ_{\max} , nm (ϵ , $\text{L mol}^{-1} \text{ cm}^{-1}$): 295 (583125), 353 (44782).

3.3.2. Synthesis of the dioxidomolybdenum(VI) complexes

(3-Methoxysalicylaldehyde-3-methoxy-

benzylhydrazonato)dimethylsulfoxidedioxidomolybdenum(VI), (1). A solution of H_2L^{3OMe} (0.300 g, 1.00 mmol), which was dissolved in 20 mL of methanol was added to a solution of $[\text{MoO}_2(\text{acac})_2]$ in 20 mL methanol. A dark orange precipitate formed immediately. DMSO was added dropwise until the precipitate was completely dissolved in the solution. The reaction mixture was then refluxed for 4 h and was allowed to stand at room temperature. Orange block shaped crystals were formed after slow evaporation for 2 days. The products were filtered, washed with ethanol and dried in air.

Yield: 0.17 g, 35%. Molar conductance (10^{-3} M DMF): $6 \Omega^{-1} \text{ cm}^2 \text{ mol}^{-1}$. Anal.Cal. for $C_{18}H_{20}MoN_2O_7S$ ($504.39 \text{ g mol}^{-1}$); C, 42.86; H, 4.00; N, 5.55; S, 6.36. Found: C, 42.92; H, 4.09; N, 5.45; S, 6.31. IR (KBr) ν_{\max} , cm^{-1} : $\nu(\text{C=N})$ 1610, $\nu(\text{C}_{\text{aro-O}})$ 1523, $\nu(\text{N-N})$ 1180, $\nu(\text{C-O})$ 1256, $\nu_{\text{asym}}(\text{cis-MoO}_2)$ 931, $\nu_{\text{sym}}(\text{cis-MoO}_2)$ 896. $^1\text{H NMR}$ (400 MHz, $\text{DMSO-}d_6$, Me_4Si , ppm) δ : 3.818 (s, 3H, methoxy), 3.827 (s, 3H, methoxy), 7.028-8.250 (m, 7H, aromatic), 8.914 (s, 1H, HC=N). UV/vis (DMF) λ_{\max} , nm (ϵ , $\text{L mol}^{-1} \text{ cm}^{-1}$): 322 (23150), 452 (8129).

Similar procedure was applied for the preparation of the complexes **2** and **3**.

(4-Methoxysalicylaldehyde-3-methoxy-

benzylhydrazonato)dimethylsulfoxidedioxidomolybdenum(VI), (2). Yield: 0.16 g, 32%. Molar conductance (10^{-3} M DMF): $12 \Omega^{-1} \text{ cm}^2 \text{ mol}^{-1}$. Anal.Cal. for $C_{18}H_{20}MoN_2O_7S$ ($504.39 \text{ g mol}^{-1}$); C, 42.86; H, 4.00; N, 5.55; S, 6.36. Found: C, 42.85; H, 4.04; N, 5.59; S, 6.35. IR (KBr) ν_{\max} , cm^{-1} : $\nu(\text{C=N})$ 1610, $\nu(\text{C}_{\text{aro-O}})$ 1523, $\nu(\text{N-N})$ 1180, $\nu(\text{C-O})$ 1256, $\nu_{\text{asym}}(\text{cis-MoO}_2)$ 931, $\nu_{\text{sym}}(\text{cis-MoO}_2)$ 896. $^1\text{H NMR}$ (400 MHz, $\text{DMSO-}d_6$, Me_4Si , ppm) δ : 3.824 (s, 3H, methoxy), 3.817 (s, 3H, methoxy), 6.545-7.648 (m, 7H, aromatic), 8.846 (s, 1H, HC=N). UV/vis (DMF) λ_{\max} , nm (ϵ , $\text{L mol}^{-1} \text{ cm}^{-1}$): 315 (22145), 421 (7120).

(5-Methoxysalicylaldehyde-3-methoxy

benzylhydrazonato)dimethylsulfoxidedioxidomolybdenum(VI), (3). Yield: 0.20 g, 40%. Molar conductance (10^{-3} M DMF): $8 \Omega^{-1} \text{ cm}^2 \text{ mol}^{-1}$. Anal.Cal. for $\text{C}_{18}\text{H}_{20}\text{MoN}_2\text{O}_7\text{S}$ ($504.39 \text{ g mol}^{-1}$); C, 42.86; H, 4.00; N, 5.55; S, 6.36. Found: C, 42.75; H, 4.03; N, 5.51; S, 6.32. IR (KBr) ν_{max} , cm^{-1} : $\nu(\text{C}=\text{N})$ 1610, $\nu(\text{C}_{\text{aro}}-\text{O})$ 1523, $\nu(\text{N}-\text{N})$ 1180, $\nu(\text{C}-\text{O})$ 1256, $\nu_{\text{asym}}(\text{cis-MoO}_2)$ 931, $\nu_{\text{sym}}(\text{cis-MoO}_2)$ 896. ^1H NMR (400 MHz, $\text{DMSO-}d_6$, Me_4Si , ppm) δ : 3.822 (s, 3H, methoxy), 3.774 (s, 3H, methoxy), 6.886-7.597 (m, 7H, aromatic), 8.903 (s, 1H, $\text{HC}=\text{N}$). UV/vis (DMF) λ_{max} , nm (ϵ , $\text{L mol}^{-1} \text{ cm}^{-1}$): 329 (25140), 430 (4123).

3.3.3 X-ray single crystal diffraction studies

Diffraction quality block shaped orange crystals **1**, **2** and **3** were mounted on a Bruker SMART APEXII CCD diffractometer, equipped with a graphite crystal, incident-beam monochromator and a fine focus sealed tube with Mo $\text{K}\alpha$ ($\lambda = 0.71073 \text{ \AA}$) radiation as the X-ray source. The unit cell dimensions were measured and the data collection was performed. The programs SAINT and XPREP were used for data reduction and APEX2 and SAINT were used for cell refinement [53]. Absorption corrections were carried out using SADABS based on Laue symmetry using equivalent reflections [54]. The crystal structures were solved by direct methods using SHELXS-97 and refined by full matrix least-squares refinement on F^2 using SHELXL-2014/7 [54] on a WinGX software package [55]. The molecular and crystal structures were plotted using ORTEP-3 [55] and DIAMOND version 3.2 g [56].

In all the complexes, anisotropic refinements were performed for all non-hydrogen atoms and all H atoms on C atoms were placed in calculated positions, guided by difference maps, with C–H bond distances of 0.93–0.96 \AA . H atoms were assigned as $U_{\text{iso}} = 1.2 U_{\text{eq}}$ (1.5 for Me). The reflections (0 1 0), (1 -1 1), (-1 0 1), (0 0 1), (0 4 0) and (-1 -1 1) in **2** and (1 -2 4), (0 0 1), (0 1 0), (0 -1 1), (-1 1 0) and (1 0 0) in **3** were omitted owing to bad agreement.

3.3.4. Hirshfeld surface calculations

Hirshfeld surface analysis represents a new radical and visually appealing approach for gaining additional insight into the intermolecular interactions between the molecules in the crystals. The size and shape of Hirshfeld surface allows the qualitative and quantitative investigation as well as visualization of intermolecular close contacts in molecular crystals. Hirshfeld surface analyses were carried out and 2D fingerprint plots were plotted using the software package Crystal Explorer 17.5 [57]. Surfaces in 3D (d_{norm}) have been mapped over a range of -0.5 \AA to 0.5 \AA , shape index (-1.0 to 1.0 \AA) and curvedness (-4.0 to 0.4 \AA) where d_{norm} function signifies the ratio covering the

distance of any surface point to the nearest interior (d_i) and exterior (d_e) atom and van der Waals radii (r^{vdw}) of the atoms. It is given by the Equation 1. The d_{norm} surfaces are mapped over a fixed color scale. The red spots over the surface indicate the intercontacts involved in hydrogen bonds [58]. The dark red spots on the d_{norm} surface arise as a result of the short interatomic contacts, i.e., strong hydrogen bonds while the other intermolecular interactions appear as light-red spots.

$$d_{norm} = \frac{d_i - r_i^{vdw}}{r_i^{vdw}} + \frac{d_e - r_e^{vdw}}{r_e^{vdw}} \quad \text{Equation 1}$$

The information generated through a Hirshfeld surface can be further quantified using two dimensional fingerprint plots [59]. The 2D fingerprint plots were displayed by using the expanded 0.6-2.8 Å view with d_e and d_i distance scales displayed on the graph axes where the frequency of occurrence of interactions (the number of points with a given (d_e , d_i) pair) are represented by the different colors blue (low frequency), green (medium) and red (high). Again, the complementary regions are visible in the FPs, where one molecule act as donor ($d_e > d_i$) and the other as an acceptor ($d_e < d_i$) [60].

3.3.5. *In vitro* cytotoxicity studies

The aroylhydrazones and their complexes were studied for their short term *in vitro* cytotoxicity using Dalton's lymphoma ascites cells (DLA). The tumour cells aspirated from the peritoneal cavity of tumour bearing mice were washed thrice with PBS (Phosphate Buffered Saline) or normal saline. Cell viability was determined by Trypan blue exclusion method. Viable cell suspension (1×10^6 cells in 0.1 mL) was added to tubes containing various concentrations of the test compounds (samples dissolved in DMSO) and the volume was made up to 1 mL using PBS control tube containing only cell suspension. These assay mixtures were then incubated for 3 hours at 37 °C. Further cell suspension was mixed with 0.1 mL of 1% trypan blue and kept for 2-3 minutes and loaded on a haemocytometer. Dead cells take up the blue colour of trypan blue while live cells do not take up the dye. The numbers of stained and unstained cells were counted separately and the % cytotoxicity was calculated using Equation 2.

$$\% \text{ Cytotoxicity} = \frac{\text{No. of dead cells}}{\text{No. of live cells} + \text{No. of dead cells}} \times 100 \quad \text{Equation 2}$$

4. Conclusion

Three new DMSO coordinated mononuclear *cis*-dioxidomolybdenum(VI) complexes of the type $[\text{MoO}_2\text{L}^R(\text{DMSO})]$ have been successfully synthesized and characterized by various physicochemical techniques and by single crystal X-ray diffraction studies. Crystallographic studies revealed that the binegative hydrazones satisfy the +2 charge of the MoO_2 moiety leading to

the formation of uncharged complexes where the molybdenum atom displays a distorted octahedral geometry. Moreover the donor solvent molecule, DMSO in the complexes is attached loosely to the MoO_2^{2+} moiety thereby making the substitution at the sixth position easy. Electrochemical study depicted the irreversible redox behaviour of these complexes. Finally all the complexes displayed a concentration dependent cytotoxic profile where the highest activity was exhibited by complex **3** with the methoxy substituent at the fifth position suggesting that the position of the substituents can also influence the cytotoxicity of the complexes. Similarly the effect of position of the substituents on the hydrazide part will be studied in due course.

Appendix A. Supplementary data

CCDC 1881036, 1881037 and 1881038 contain the supplementary crystallographic data for $[\text{MoO}_2\text{L}^{3\text{OMe}}(\text{DMSO})]$ (**1**), $[\text{MoO}_2\text{L}^{4\text{OMe}}(\text{DMSO})]$ (**2**) and $[\text{MoO}_2\text{L}^{5\text{OMe}}(\text{DMSO})]$ (**3**) respectively. These data can be obtained free of charge via www.ccdc.cam.ac.uk/conts/retrieving.html or from the Cambridge Crystallographic Data Centre, 12 Union Road, Cambridge CB2 IEZ, UK; fax: (+44) 1223-336-033; or e-mail: deposit@ccdc.cam.ac.uk.

Acknowledgement

T.M. Asha acknowledges the CSIR, New Delhi, India for the award of a Senior Research Fellowship (09/239(0510)/2015-EMR-I). The authors are thankful to the Sophisticated Analytical Instrumentation Facility, Cochin University of Science and Technology, Kochi, India for elemental analysis, ^1H NMR spectra and single crystal X-ray diffraction measurements.

References

- [1] A.A.A. Abu-Hussen, J. Coord. Chem. 59 (2006) 157.
- [2] P.B. Sreeja, M.R.P. Kurup, A. Kishore, C. Jasmine, Polyhedron 23 (2004) 575.
- [3] K. Singh, M.S. Barwa, P. Tyagi, Eur. J. Med. Chem. 41 (2006) 147.
- [4] P. Pannerselvam, R.R. Nair, G. Vijayalakshmi, E.H. Subramanian, S.K. Sridhar, Eur. J. Med. Chem. 40 (2005) 225.
- [5] S.K. Sridhar, M. Saravanan, A. Ramesh, Eur. J. Med. Chem. 36 (2001) 615.
- [6] N.A. Mathews, A. Jose, M.R.P. Kurup, J. Mol. Struct. 1178 (2019) 544.
- [7] R. Mladenova, M. Ignatova, N. Manolova, T. Petrova, I. Rashkov, Eur. Polym. J. 38 (2002) 989.
- [8] O.M. Walsh, M.J. Meegan, R.M. Prendergast, T.A. Nakib, Eur. J. Med. Chem. 31 (1996) 989.

- [9] F.A. Afkhami, G. Mahmoudi, A.A. Khandar, A. Franconetti, E. Zangarando, N. Qureshi, J. Lipkowski, A.V. Gurbanov, A. Frontera, *European J. Inorg. Chem.*, 2018 (2019) 262; G. Mahmoudi, A.A. Khandar, F.A. Afkhami, B. Mirslaw, A.V. Gurbanov, F.I. Zubkov, A. Kennedy, A. Franconetti, A. Frontera, *CrystEngComm*. 2019 (21) 108; D. Sadhukhan, M. Maiti, A. Bauza, A. Frontera, E. Garribba, C.J. Gomez-Garcia, *Inorg. Chim. Acta* 2019 (484) 95; S.K. Seth, A. Bauza, G. Mahmoudi, V. Stilnovic, E. Lopez-Torres, G. Zaragoza, A.D. Keramidas, A. Frontera, *CrystEngComm*. 2018 (20) 5033.
- [10] Z. Travnicek, M. Malon, Z. Sindelar, K. Dolezal, J. RoIcik, V. Krystof, M. Strnad, J. Marek, *J. Inorg. Biochem.* 84 (2001) 23.
- [11] M. Sonmez, I. Berber, E. Akbas, *Eur. J. Med. Chem.* 41 (2006) 101.
- [12] J.M. Berg, R.H. Holm, *J. Am. Chem. Soc.* 107 (1985) 925.
- [13] R.H. Holm, *Chem. Rev.* 87 (1987) 1401.
- [14] R.H. Holm, *Coord. Chem. Rev.* 100 (1990) 183.
- [15] S. Purohit, A.P. Koley, L.S. Prasad, P.T. Manoharan, S. Ghosh, *Inorg. Chem.* 28 (1989) 3735.
- [16] A. Rana, R. Dinda, P. Sengupta, S. Ghosh, L.R. Falvello, *Polyhedron* 21 (2002) 1023; M. E. Judmaier, C. Holzer, M. Volpe, N.C. Mosch-Zanetti, *Inorg. Chem.* 51 (2012) 9956; c) T.M. Asha, M.R.P. Kurup, *J Chem Crystallogr.*, 2018, <https://doi.org/10.1007/s10870-018-0756-9>.
- [17] O.A. Rajan, A. Chakravorty, *Inorg. Chem.* 20 (1981) 660.
- [18] M.M. Abu-omar, A. Loaiza, N. Hontzeas, *Chem. Rev.* 105 (2005) 2227.
- [19] J. Topich, *Inorg. Chem.* 20 (1981) 3704.
- [20] E.I. Stiefel, *Science* 272 (1996) 1599.
- [21] E.I. Stiefel, in: S. J. Lippard (Ed.), *Progress in Inorganic Chemistry*, John Wiley & Sons Inc, New York 22 (1977) 1.
- [22] A. Majumdar, S. Sarkar, *Coord. Chem. Rev.* 255 (2011) 1039.
- [23] R.H. Holm, E.I. Solomon, A. Majumdar, A. Tenderholt, *Coord. Chem. Rev.* 255 (2011) 993.
- [24] S. Metz, W. Thiel, *Coord. Chem. Rev.* 255 (2011) 1085.
- [25] R. Hille, *Chem. Rev.* 96 (1996) 2757.
- [26] D. Collison, C.D. Garner, J.A. Joule, *Chem. Soc. Rev.* 25 (1996) 25.
- [27] J. Liimatainen, A. Lehtonen, R. Sillanpaa, *Polyhedron* 19 (2000) 1133.
- [28] J.P. Cao, L.L. Zhou, L.Z. Fu, J.X. Zhao, H.X. Lu, S.Z. Zhan, *Catal. Commun.* 57 (2014) 1.
- [29] J. Zhang, P. Jiang, Y. Shen, W. Zhang, X. Li, *Microporous Mesoporous Mater* 206 (2015) 161.
- [30] S. Rayati, N. Rafiee, A. Wojtczak, *Inorg. Chim. Acta* 386 (2012) 27.
- [31] E. Zamanifar, F. Farzaneh, J. Simpson, M. Maghami, *Inorg. Chim. Acta* 414 (2014) 63.

- [32] T.M. Asha, M.R.P. Kurup, *Inorg. Chim. Acta* 483 (2018) 44.
- [33] W.J. Geary, *Coord. Chem. Rev.* 7 (1971) 81.
- [34] M.M. Fousiamol, M. Sithambaresan, V.A. Smolenski, J.P. Jasinski, M.R.P. Kurup, *Polyhedron* 141 (2018) 60.
- [35] A. Aravindakshan, B. Joseph, U.L. Kala, M.R.P. Kurup, *Polyhedron* 123 (2017) 206.
- [36] B.S. Garg, M.R.P. Kurup, S.K. Jain, Y.K. Bhoon, *Transit Met. Chem.* 16 (1991) 111; M. Kuriakose, M.R.P. Kurup, E. Suresh, *Polyhedron* 26 (2007) 2713.
- [37] R.A. Lal, A. Kumar, J. Chakraborty, S. Bhaumik, *Transit. Met. Chem.* 26 (2001) 557.
- [38] S. Roy, Saswati, S. Lima, S. Dhaka, M.R. Maurya, R. Acharyya, C. Eagle, R. Dinda, *Inorg. Chim. Acta* 474 (2018) 134.
- [39] A.P. Koley, S. Purohit, S. Ghosh, L.S. Prasad, P.T. Manoharan, *J. Chem. Soc. Dalton Trans.*, 0 (1988) 2607.
- [40] R. Dinda, P. Sengupta, S. Ghosh, W.S. Sheldrich, *Eur. J. Inorg. Chem.*, 2003 (2003) 363.
- [41] R. Dinda, S. Ghosh, L.R. Falvello, M. Tomas, T.C.W. Mak, *Polyhedron* 25 (2006) 2375.
- [42] E.B. Seena, M.R.P. Kurup, *Polyhedron* 26 (2007) 3595.
- [43] P. Nag, R. Bohra, R.C. Mehrotra, R. Ratnani, *Tran. Met. Chem.* 27 (2002) 321; J.H. Enemark, J.J.A. Cooney, J.J. Wang, R.H. Holm, *Chem. Rev.* 104 (2004) 1175.
- [44] M.J. Turner, J.J. McKinnon, S.K. Wolf, D.J. Grimwood, P.R. Spackman, D. Jayatilaka, M.A. Spakman, *Crystal Explorer 17.5*, 2017, University of West Australia.
- [45] S.S. Sreejith, N. Mohan, M.R.P. Kurup, *J. Mol. Struc.* 1145 (2017) 170.
- [46] A.Y. Meyer, *Chem. Soc. Rev.* 15 (1986) 449.
- [47] P.P. Devi, D. Kalaivania, *Acta Cryst.* E72 (2016) 570.
- [48] P. Venkatesan, S. Thamotharan, A. Illangovan, H. Liang, T. Sundius, *Spectrochim. Acta Part A* 153 (2016) 625.
- [49] M. Malecka, E. Budzisz, *CrystEngComm.* 16 (2014) 6654.
- [50] G. Mahmoudi, A. Bauza, A. Rhodriguez-Dieguez, P. Garczarek, W. Kaminsky, A. Fronter, *CrystEngComm.* 18 (2016) 102.
- [51] Y. Li, C.G. Zhang, L.Y. Cai, Z.X. Wang, *J. Coord. Chem.* 66 (2013) 3100.
- [52] C.F. Matta, J. Hernandez- Trujillo, T.H. Tang Dr, R.F.W. Bader, *Chem. Eur. J.* 9 (2003) 1940.
- [53] SMART and SAINT, Area Detector Software Package and SAX Area Detector Integration Program, Bruker Analytical X-ray, Madison, WI, USA, 1997.
- [54] SADABS, Area Detector Absorption Correction Program; Bruker Analytical X-ray; Madison, WI, USA, 1997.
- [55] G.M. Sheldrick, *Acta Crystallogr.* C71 (2015) 3.

- [56] L.J. Farrugia, *J. Appl. Crystallogr.* 45 (2012) 849.
- [57] K. Brandenburg, *Diamond version 3.2g*, Crystal Impact, GbRBonn, Germany, 2011.
- [58] A. Wang, B.M. Craven, *J. Pharm. Sci.* 68 (1979) 361; M. A. Spackman, P. G. Byrom, *Chem. Phys. Lett.* 267 (1997) 215; M.A. Spackman, D. Jayatilaka, *Cryst. Eng. Comm.* 11 (2009) 19; S. K. Seth, D. Sarkar, A.D. Jana, T. Kar, *Cryst. Growth Des.* 11 (2011) 4837.
- [59] J.J. Mckinnon, M. A. Spackman, A.S. Mitchell, *Acta Cryst. B*60 (2004) 627.
- [60] S.S. Sreejith, A. Nair, V.A. Smolenski, J.P. Jasinski, M.R.P. Kurup, *Inorg. Chim. Acta* 469 (2018) 264; S. K Wolff, D.J. Grimwood, J.J. McKinnon, M.J. Turner, D. Jayatilaka, M.A. Spakman, *Crystal Explorer (Version 3.1)* 2012.

Table 1. Results of thermogravimetric analysis of complexes **1-3**

Compound	Temperature range (°C)	Weight loss observed (Calculated)%	Molecules lost	End Residue
Complex 1	(a) 200-240	14.70 (15.46)	DMSO	MoO ₃
	(b) 270-290	33.42 (32.31)	Hydrazone fragment ^[a]	
Complex 2	(a) 150-210	15.61(15.46)	DMSO	MoO ₃
	(b) 270-310	31.17 (32.31)	Hydrazone fragment ^[a]	
Complex 3	(a) 170-205	17.90 (15.46)	DMSO	MoO ₃
	(b) 270-310	32.01 (32.31)	Hydrazone fragment ^[a]	

^[a] = CH₃O-C₆H₄-CONN

Table 2. Cyclic voltammetry results for the studied compounds

Compound	E _{pc} ^[a]
H ₂ L ^{3OMe}	-0.458
H ₂ L ^{4OMe}	-1.233
H ₂ L ^{5OMe}	-1.479
Complex 1	-0.331, -0.894
Complex 2	-0.190
Complex 3	-0.198

^[a]Solvent: DMF; working electrode: platinum; auxiliary electrode: platinum; reference electrode: Ag/AgCl; supporting electrolyte: 0.1 M TEAP; scan rate: 100 mV/ s. E_{pc} is the cathodic peak potential.

Table 3. Crystal data and refinement details of **1-3**.

Parameters	[MoO ₂ L ^{3OMe} (DMSO)] (1)	[MoO ₂ L ^{4OMe} (DMSO)] (2)	[MoO ₂ L ^{5OMe} (DMSO)] (3)
Empirical formula	C ₁₈ H ₂₀ MoN ₂ O ₇ S	C ₁₈ H ₂₀ MoN ₂ O ₇ S	C ₁₈ H ₂₀ MoN ₂ O ₇ S
Formula weight	504.36	504.36	504.36
Crystal system	Triclinic	Triclinic	Triclinic
Space group	$P\bar{1}$	$P\bar{1}$	$P\bar{1}$
Cell parameters			
a (Å)	8.5060(6)	7.5269(6)	8.4972(3)
b (Å)	10.7073(6)	10.8302(10)	10.6204(4)
c (Å)	12.0592(7)	13.5388(13)	12.5081(5)
α (°)	69.403(2)	98.681(4)	110.271(2)
β (°)	82.375(3)	103.478(4)	102.808(2)
γ (°)	87.739(3)	102.701(4)	96.366(2)
Volume(V) (Å ³)	1018.98(11)	1022.94(16)	1010.55(7)
Z	2	2	2
Calculated density (ρ)(Mg m ⁻³)	1.644	1.637	1.658
Absorption coefficient, μ (mm ⁻¹)	0.789	0.789	0.795
F(000)	512	512	512
Crystal size (mm ³)	0.35 x 0.30 x 0.30	0.30 x 0.20 x 0.20	0.50 x 0.30 x 0.20
θ (°)	3.107 - 28.179	2.781-28.199	2.654- 28.315
Limiting indices	-11 \leq h \leq 10 -12 \leq k \leq 14 -16 \leq l \leq 16	-9 \leq h \leq 7 -14 \leq k \leq 14 -17 \leq l \leq 17	-11 \leq h \leq 10 -13 \leq k \leq 14 -16 \leq l \leq 16
Reflections collected / unique reflections (R_{int})	7643 / 5017 , (R_{int} = 0.0139)	8072 / 4559 , (R_{int} = 0.0166)	16659/4899 , (R_{int} = 0.0214)
Completeness to θ	95.6	99.2	99.8
Absorption correction	Semi-empirical from equivalents	Semi-empirical from equivalents	Semi-empirical from equivalents
Maximum and minimum transmission	0.798 and 0.761	0.790 and 0.755	0.791 and 0.757
Data / restraints / parameters	4693 / 0 / 266	4559 / 0 / 266	4899 / 0 / 266
Goodness-of-fit(GOF) on F ²	1.108	1.092	1.046
Final R indices [$I > 2\sigma(I)$]	$R_1 = 0.0320$, $wR_2 = 0.0739$	$R_1 = 0.0223$, $wR_2 = 0.0587$	$R_1 = 0.0284$, $wR_2 = 0.0689$
R indices (all data)	$R_1 = 0.0378$, $wR_2 = 0.0797$	$R_1 = 0.0262$, $wR_2 = 0.0616$	$R_1 = 0.0336$, $wR_2 = 0.0724$
Largest difference peak and hole (eÅ ⁻³)	0.738 and -0.679	0.335 and -0.435	1.421 and -0.499

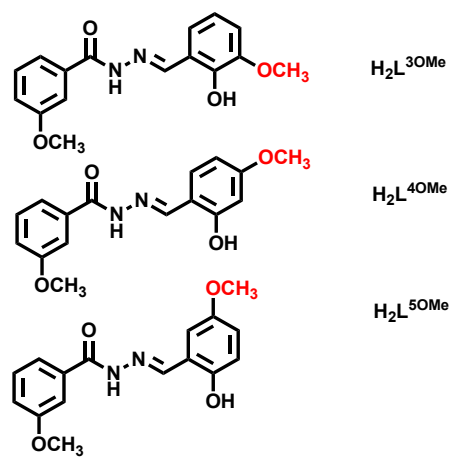
$$R_1 = \sum ||F_o| - |F_c|| / \sum |F_o|, wR_2 = [\sum w(F_o^2 - F_c^2)^2 / \sum w(F_o^2)^2]^{1/2}$$

Table 4. Selected bond lengths (Å) and bond angles (°) of compounds **1–3**.

Bond Lengths	1	2	3
C(1)–O(1)	1.350(3)	1.347(2)	1.359(2)
C(8)–O(3)	1.325(3)	1.334(2)	1.330(2)
C(15)–O(2)	1.427(4)	1.430(3)	1.408(4)
C(16)–O(4)	1.405(5)	1.419(3)	1.417(4)
C(7)–N(1)	1.285(3)	1.294(2)	1.282(3)
C(8)–N(2)	1.298(3)	1.296(2)	1.289(3)
N(1)–N(2)	1.394(3)	1.403(2)	1.403(2)
N(1)–Mo(1)	2.232(2)	2.227(15)	2.238(17)
O(3)–Mo(1)	2.020(3)	1.998(13)	1.998(14)
O(5)–Mo(1)	1.706(18)	1.718(13)	1.707(16)
O(6)–Mo(1)	1.694(19)	1.697(15)	1.694(17)
O(7)–Mo(1)	2.306(19)	2.323(15)	2.311(15)
Bond Angle			
O(6)–Mo(1)–O(5)	106(10)	105(17)	105.09(9)
O(6)–Mo(1)–O(1)	97.99(9)	99.05(7)	98.91(8)
O(5)–Mo(1)–O(1)	105.24(9)	103.91(6)	103.73(7)
O(6)–Mo(1)–O(3)	97.30(9)	95.75(7)	97.32(8)
O(5)–Mo(1)–O(3)	94.90(8)	95.56(6)	96.39(7)
O(1)–Mo(1)–O(3)	150.06(8)	151.42(6)	149.76(6)
O(6)–Mo(1)–N(1)	92.17(9)	95.78(7)	92.84(8)
O(5)–Mo(1)–N(1)	158.66(9)	156.91(7)	159.82(8)
O(1)–Mo(1)–N(1)	82.08(8)	81.97(6)	82.09(6)
O(3)–Mo(1)–N(1)	71.75(8)	72.29(5)	71.76(6)
O(6)–Mo(1)–O(7)	167.74(9)	169.59(6)	168.92(7)
O(5)–Mo(1)–O(7)	85.92(9)	84.95(6)	85.92(8)
O(1)–Mo(1)–O(7)	79.42(7)	80.71(6)	79.22(6)
O(3)–Mo(1)–O(7)	80.19(7)	80.39(6)	79.97(6)
N(1)–Mo(1)–O(7)	75.62(7)	73.85(5)	76.10(6)

Table 5. Percentage of cell death for the aroylhydrazones and their molybdenum complexes.

Drug Concentration $\mu\text{g/ mL}$	Percentage cell death (DLA) %					
	$\text{H}_2\text{L}^{3\text{OMe}}$	1	$\text{H}_2\text{L}^{4\text{OMe}}$	2	$\text{H}_2\text{L}^{5\text{OMe}}$	3
200	8	25	9	24	8	32
100	6	12	6	16	7	22
50	2	8	4	8	4	16
20	0	2	0	4	1	10
10	0	0	0	0	0	4



Scheme 1: Structures of the aroylhydrazones.

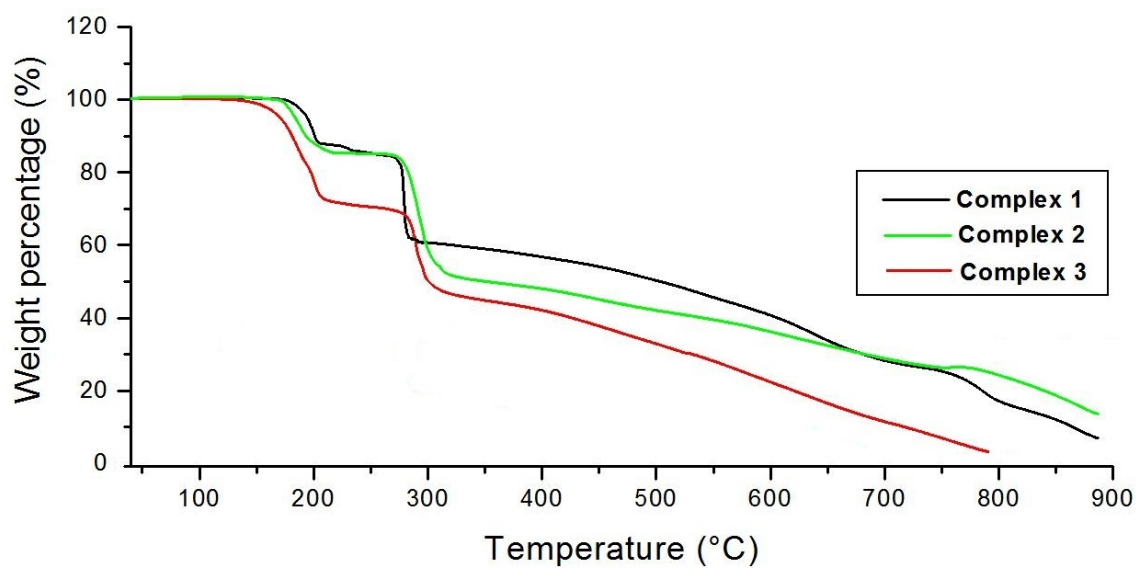


Figure 1: Thermograms of complexes 1-3.

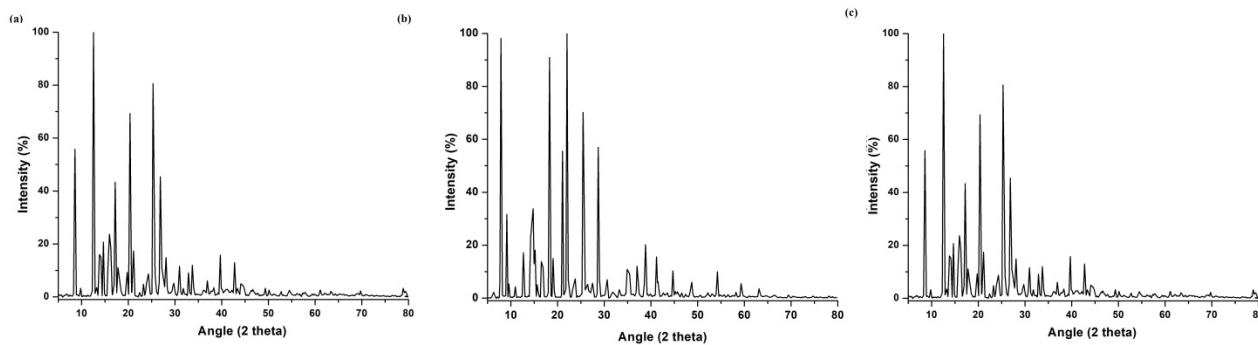
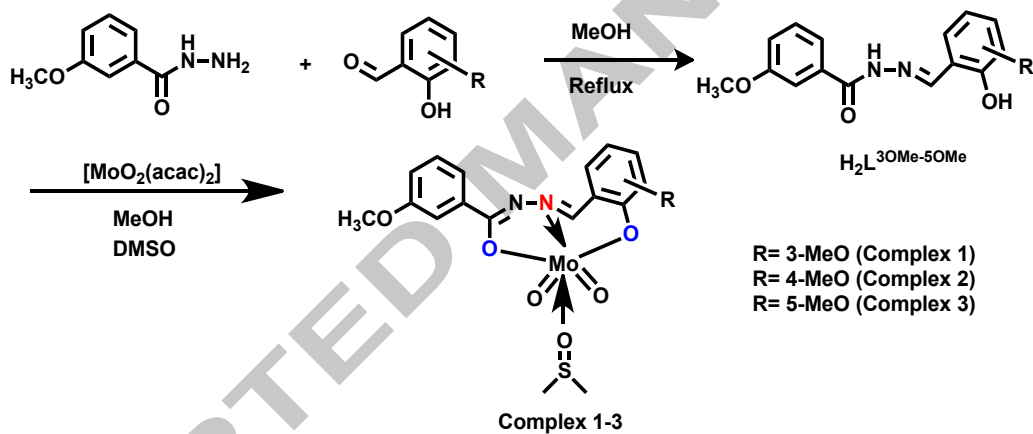


Figure 2: Powder XRD diffraction pattern of complexes 1-3 (a-c).



Scheme 2: Synthesis of the aroylhydrazone ligands and the molybdenum complexes.

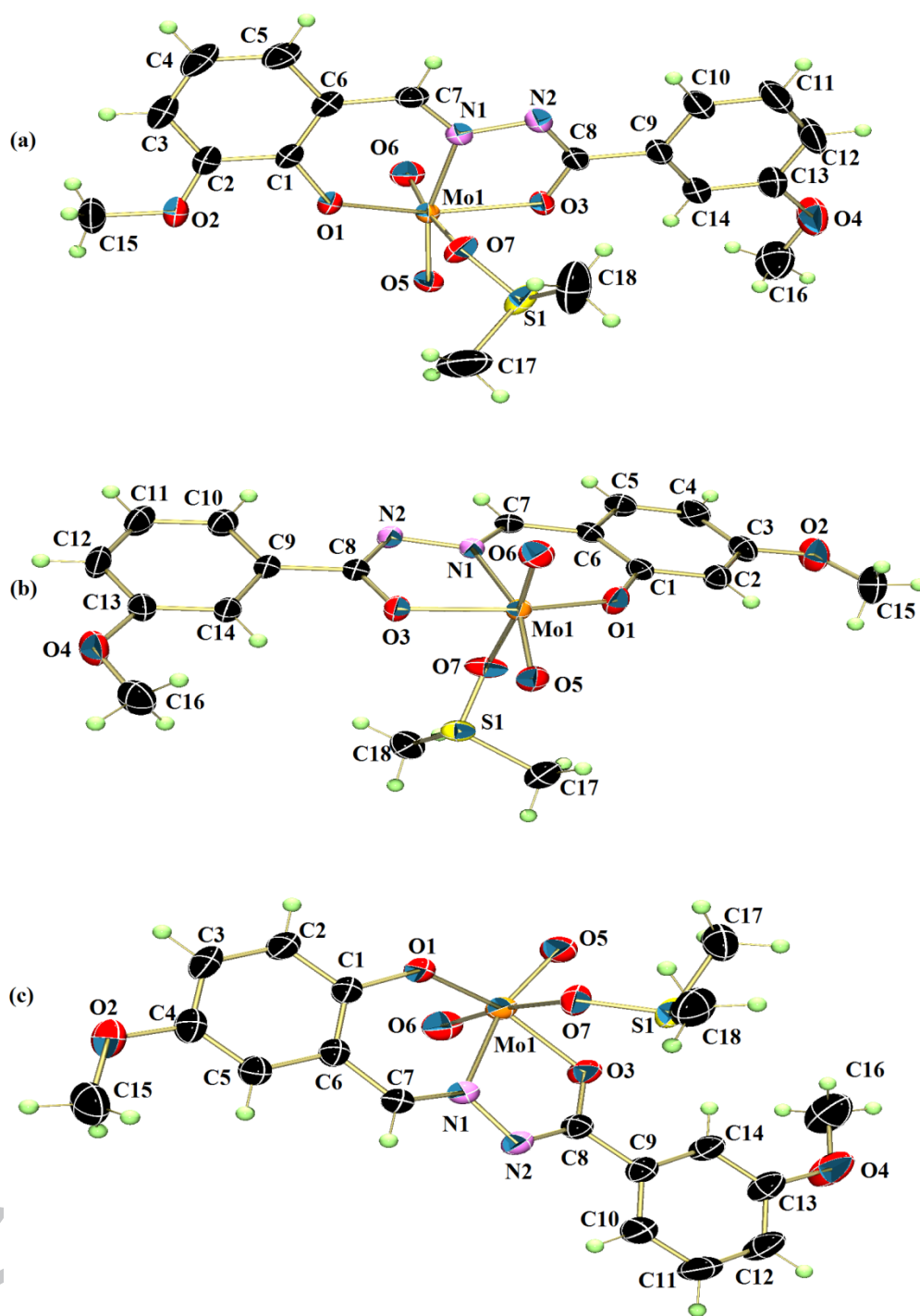


Figure 3: ORTEP plot of [MoO₂L^{30Me}(DMSO)] (1) (a), [MoO₂L^{40Me}(DMSO)] (2) (b) and [MoO₂L^{50Me}(DMSO)] (3) (c) along with atom numbering scheme of the non-hydrogen atoms. Displacement ellipsoids are drawn at 50% probability.

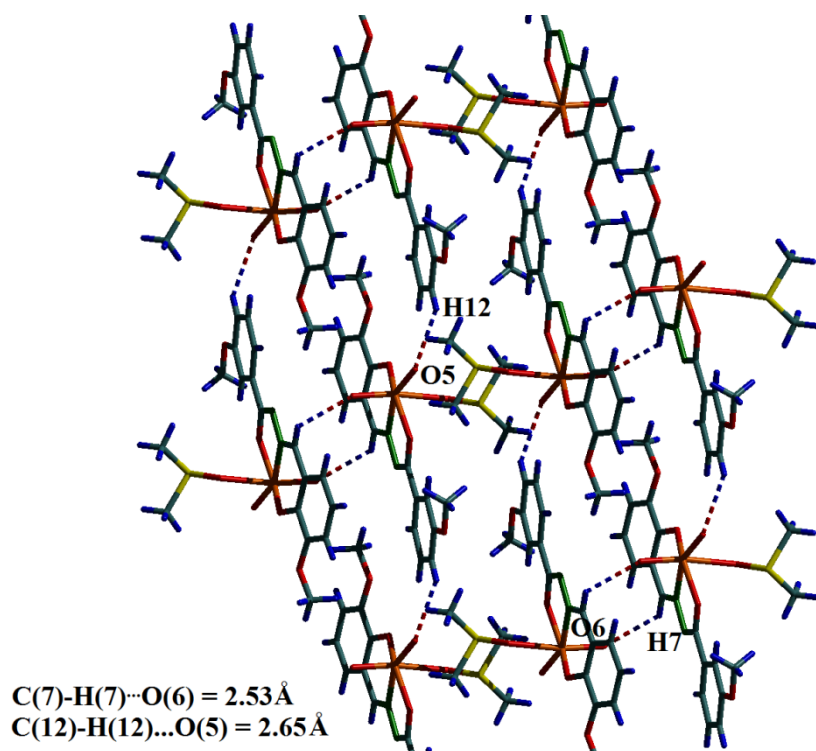


Figure 4: Diagram depicting major hydrogen bonding interactions in $[\text{MoO}_2\text{L}^{3\text{OMe}}(\text{DMSO})]$ (1).

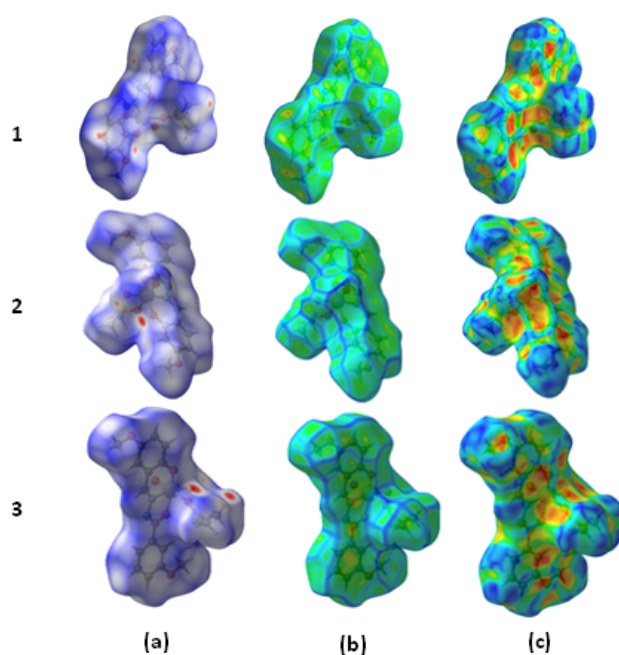


Figure 5: (a) Hirshfeld surface mapped with d_{norm} (color scale from -0.1203 to 1.2821 (for 1 and 2; color scale from -0.2153 to 1.4542 (for 3)), (b) shape index and (c) curvedness for the compounds 1-3.

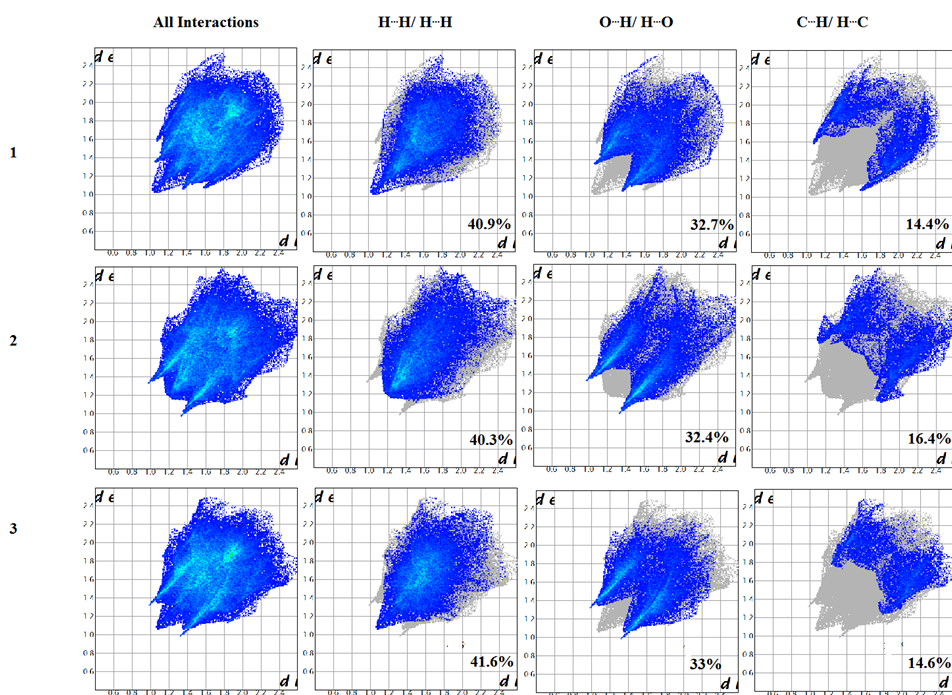


Figure 6: 2D fingerprint plots with d_e and d_l ranging from 1 to 2.8 Å for **1-3** and their major decomposition plots.

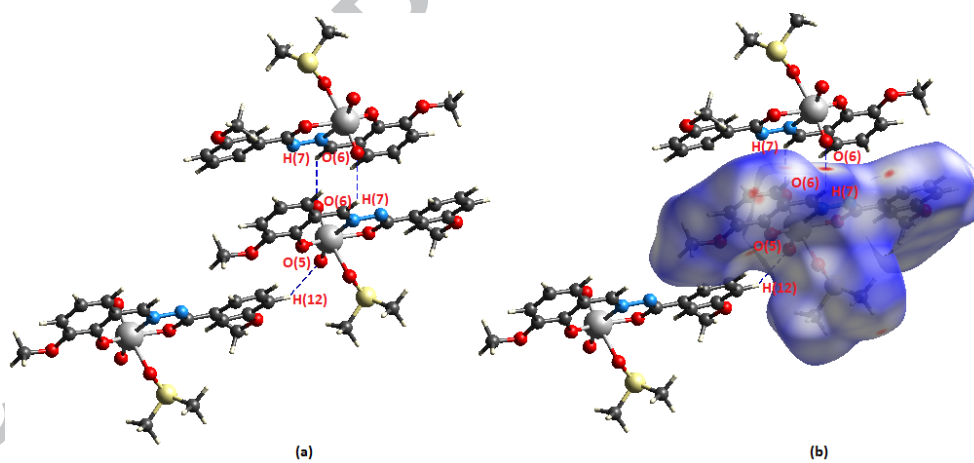


Figure 7: (a) Non-classical hydrogen bonding interactions present in **1** involving C7–H7 \cdots O2 and C12–H12 \cdots O5, (b) viewing the same short contacts in Hirshfeld surface with external molecules.

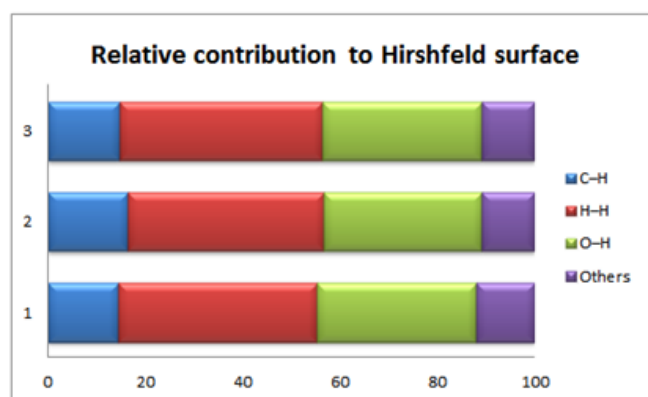


Figure 8: Percentage contributions to the Hirshfeld surface area for the various close intermolecular contacts for molecules.

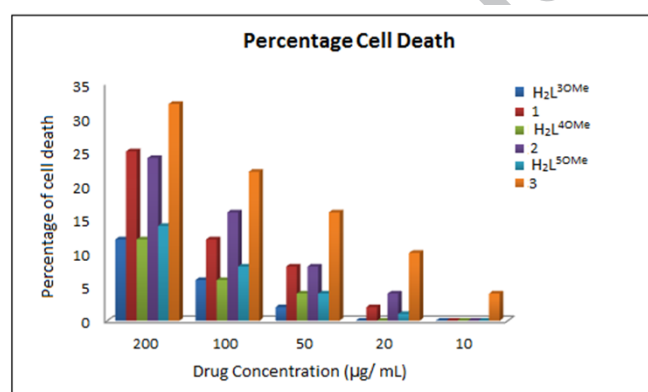


Figure 9: Cytotoxicity profiles of the aroylhydrazones and their molybdenum complexes.

Three new DMSO coordinated dioxidomolybdenum(VI) complexes of aroylhydrazones were synthesized and spectral and structural studies were done. The *in vitro* cytotoxicity of the aroylhydrazone ligands and their molybdenum complexes against lymphoma acsites cell line demonstrated that the complexes are more cytotoxic than their corresponding ligands.

ACCEPTED MANUSCRIPT

DMSO coordinated dioxidomolybdenum(VI) complexes chelated with 3-methoxybenzhydrazone related ligands: synthesis, structural studies and *in-vitro* cytotoxicity

T. M. Asha and M. R. P. Kurup

Graphical Abstract

